Proceedings of the International Conference on Industrial Engineering and Operations Management

Publisher: IEOM Society International, USA DOI: 10.46254/BA08.20250325
Published: December 20, 2025

Effect of Notch Geometry on Vortex-Induced Vibration: A Numerical Study

Muhammad Jawad Zin Noor
Department of Mechanical Engineering
Khulna University of Engineering & Technology
Khulna, Bangladesh
jawadzinnoor.kuet.2023@gmail.com

Joy Ganguly
Department of Mechanical Engineering
Khulna University of Engineering & Technology
Khulna, Bangladesh
joyganguly1705@gmail.com

Teertha Toran Chakraborty
Department of Mechanical Engineering
Khulna University of Engineering & Technology
Khulna, Bangladesh
tirtho2603@gmail.com

Abstract

The study presents a numerical investigation of the effect of notch geometry on VIV for fluid flow over a circular cylinder. Three types of notches were simulated and compared against a smooth cylinder: rectangular notches, semi-circular notches, and triangular notches. All the notches had an opening of 0.1D but with different geometries. The body was subjected to a fluid (air) flow at 10,000 Re. The results showed that the presence of notches significantly increased the VIV response of the cylinder. Triangular notches induce the strongest increase in lift forces and result in a 20.80% increase in deformation. A Strouhal number closer to 0.2 indicates that notches aid in the shedding of vortices of the flow, and flow around triangular notches has the highest periodic vortices generation. These findings provide a geometric selection framework for design optimization, demonstrating how specific notch profiles can be utilized to modulate flow-induced loads and tune the structural response of cylindrical components in cross-flow environments.

Keywords

VIV, Fluid Structure Interaction, CFD, RANS, ALE, ANSYS, System Coupling, Notched VIV, Transient FSI.

1. Introduction

Vortex-Induced Vibrations (VIV) are the oscillatory motions of a body in a fluid flow that are caused by the alternating lift forces generated by the vortex shedding. This phenomenon occurs when a cylinder or similar structure is subjected to a fluid flow, and it can result in severe vibrations and even structural damage.

© IEOM Society International

VIV is a complex process involving several fluid-structure interactions and aerodynamic phenomena, and it must be considered in a wide range of engineering applications, such as offshore oil platforms, bridges, and pipelines. The interaction between the fluid flow and the body, which leads to the release of vortices and the formation of alternating lift forces, is the fundamental mechanism behind VIV. These lift forces induce oscillations in the body, leading to the development of VIV. The frequency and amplitude of the vibrations rely on many variables, including fluid velocity, body size and shape, and the existence of flow disturbances or structural features.

Higher frequency and amplitude vibrations can result in very high magnitudes of cyclic stress, which can lead to devastating rates of fatigue failure over time. Especially, if lock-in phenomenon happens. In that instance, the frequency of the oscillating motion of the object matches the natural frequency of the oscillating body, thus resulting in resonance. Such instances are detrimental to the integrity of the structure. Different methods have been proposed and studied for the suppression of such a phenomenon. Both active and passive methods are used in practice. Between sthem, passive means are more sustainable, since they require no external energy output. In this study, such a passive means will be investigated, where a notch will be created on the periphery of the cylindrical structure, and its effect on VIV will be investigated.

1.1 Problem Description

When a fluid flows past a blunt object, like a circular cylinder, vortices are formed at the wake of the cylinder and are shed periodically from either side, generating time-varying non-uniform pressure distribution around the cylindrical structure. The cylinder's force components vary periodically. Vortex shedding generates in-line and cross-flow forces that vibrate the structure. The subsequent study will examine the impact of notch geometry on the various properties of vortex-induced vibrations. Previous research has shown that different discontinuities on the surface of the bluff body in unidirectional fluid flow have distinct effects on the vortex shedding characteristics and the produced vortex features.

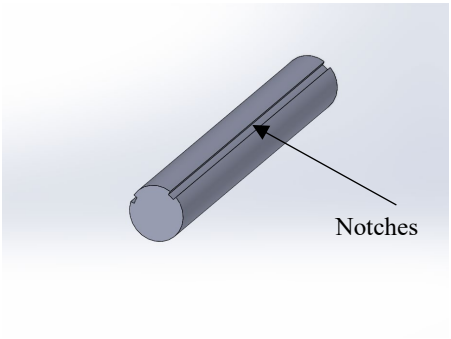

Figure 1. Geometry of the bluff body.

The bluff body is a solid cylinder with longitudinal notches as shown in Figure 1. It is placed vertically in the flow domain. The orientation is shown below in Figure 2. The direction of the fluid flow is shown with black arrows. The vertical cylinder has one end fixed, whilst the other end is free moving.

© IEOM Society International

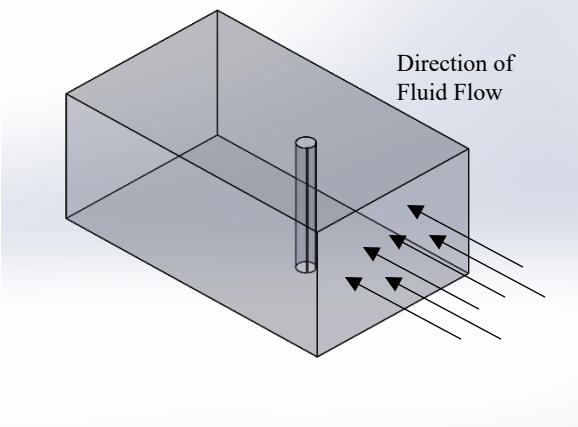

Figure 2. Orientation of flow compared to the bluff body.

The moving fluid is continuously deforming the bluff body, whilst the deformation of the bluff body is also affecting the surrounding fluid flow. To observe their effect on each other numerically, the characteristics of the solid as well as the fluid portion must be calculated simultaneously.

1.2 Objectives

The general objective is to simulate unidirectional fluid flow over different notched vertical cylinder. The specific objectives are:

- To develop a numerical model to simulate the fluid flow and structural characteristics.
- To compare VIV characteristics for different geometries using the developed model.

2. Literature Review

Vortex-induced vibration (VIV) occurs when shedding vortices (a von Kármán vortex street) exert oscillatory forces in the direction perpendicular to the flow and the structure of a cylinder. If the structure is not fixed, these forces cause it to oscillate. The vortex-shedding frequency of fixed cylinders is related to the dimensionless Strouhal number. The Strouhal number is defined as $S_t = Df_s/U$; where f_s is the predominant frequency of vortex shedding. U is the constant flow velocity, and D is the cylinder's diameter.

In the highly specialized topic of vortex-induced vibrations (VIVs), oscillations, computational fluid dynamics (CFD), acoustic performance, wavelet transformations, challenging demodulation analysis, and statistics are all taken into consideration. Engines, marine cables, bridges, transmission cables, stacks, control surfaces of aircraft, towed cables, offshore marine structures, heat exchangers, thermos-walls, petroleum industry drilling and production risers, buoyancy and spar hulls, cable laying, conduits, parts of coated frameworks, and other hydraulic and hydroacoustic applications. Our knowledge of the kinematics of VIV has significantly improved in the last ten years, both computationally and empirically. Contrary to popular belief, VIV is not a minute disturbance superimposed on a mean steady-state motion. For a wide range of Reynolds numbers, it is discovered by Chen et al. that the Strouhal number is nearly constant at 0.2. This range of Reynolds numbers, 300-2×10^5, is commonly referred to as the subcritical range (ShoeiSheng Chen, 1987).

Parkinson et al. experimentally measured and studied the alternating forces working on a bluff body in unidirectional fluid flow for offshore marine applications (Parkinson, 1989). Bearman experimentally measured and studied oscillations resulting from the unidirectional fluid flow on a bluff body (Bearman, 1984).

The literature is well-researched on VIV's effects on engineering. For research focusing on the VIV of large structures, structures like towering buildings, chimneys, stacks, and long-span bridges create noticeable vibrations when exposed to fluid flow (Matsumoto et al., 2001; Okajima & Kiwata, 2019).

© IEOM Society International

The issue is made worse by the length and greater flexibility of some of these structures. VIV of long, slender structures like pipelines, risers, tendons, and spar platforms present a challenge to engineering designers in offshore applications (Amabile, 2004). Included are a few illustrations of foundational research on the nature of the VIV of marine structures (Vandiver, 1993). Assessment and suppression of VIV have both been the subject of extensive research (Hussein & Baz, 2008).

Numerical simulations on VIV can provide valuable insights into the behavior of fluid-structure interactions and can be used to optimize the design of structures subject to VIV. They can also be used to validate experimental results and to study the effects of different parameters, such as the Reynolds number, the mass ratio, and the structural properties of the system.

Many attempts have also been made to numerically simulate the VIV reactions of rigid cylinders positioned elastically. The turbulent flow around the cylinder is typically modeled using four computational approaches: Direct Numerical Simulation (DNS), Large Eddy Simulation (LES), Detached Eddy Simulation (DES), and Reynolds-Averaged Navier-Stokes (RANS) Simulation. The various turbulence modeling methodologies have been evaluated by Argyropoulos and Markatos (Argyropoulos & Markatos, 2015), who also provided a summary of the benefits and drawbacks of each approach. In comparison to RANS simulations, DNS, LES, and DES approaches typically yield more accurate findings. On the other hand, RANS-based codes offer the optimum compromise between accuracy and computational expense. As a result, it is more useful for fluid flow simulations, and RANS programs have been extensively employed in literature (Zhao et al., 2014a).

However, it is important to note that numerical simulations on VIV can be computationally expensive and require significant computational resources. Additionally, the accuracy of the simulations depends on the quality of the numerical models used, and the results should be validated against experimental data to ensure accuracy. One common approach to simulating VIV is to use an unsteady Reynolds-Averaged Navier-Stokes (URANS) solver, which can accurately model the unsteady behavior of the flow and the structure. The simulation domain is typically divided into a fluid domain and a solid domain, and the interaction between the fluid and the structure is modeled using boundary conditions.

Numerous studies have looked into VIV in cylinders that are round, but the majority of them used low Re and low mass ratios. Placzek et al. (Placzek et al., 2009) studied VIV at a low mass ratio and low Re (Re = 100) using the 2-dimensional RANS code. The 2-dimensional RANS code at Re = 100 successfully caught the mode of vortex shedding. Zhao et al. used 3-dimensional Navier-Stokes equations to examine the VIV phenomena with Reynolds numbers Re = 150 to 1000. The authors concluded that the 2-dimensional RANS equation outperforms the 2-dimensional Navier—Stokes equation in terms of analyzing VIV behavior in a turbulent environment(Zhao et al., 2014b). The Smagorinksy—Lilly subgrid-scale model and LES code were used by Khan et al. to analyze the wake characteristics and hydrodynamics at Re = 3900(Khan et al., 2016).

Islam, Manzoor, and Zhou quantitatively investigated the causes of the decrease in vortex shedding and accompanying drag forces for flow around a square cylinder at Reynolds numbers between 80 and 200(Islam et al., 2017). The effect of the aspect ratio of a rectangular cylinder on the vortex mode, fluid forces, and vortex-shedding frequency at Re = 100 to 250 was examined by Islam et al. using the incompressible Boltzmann method(Islam et al., 2012). The dynamic and wake modes of a sphere under VIV at Re = 300 to 100 at a low mass ratio were studied by Behara and Sotiropoulos (Behara & Sotiropoulos, 2016).

The decreased velocity (U_r) ranged from 0 to 13 when the investigation was conducted. The authors came to the conclusion that Re has a significant influence on the sphere's wake modes and trajectory. With the same shear flow parameter, Liangjie et al. explored VIV at various Re and found that the multimodal phenomena are more important at high Re. The main vibration mode was seen at the natural frequency's highest order mode(Liangjie et al., 2014). Based on LES using 2-dimensional and 3-dimensional models at Re = 24,000, Tutar and Holdo's investigation was conducted (Tutar & Holdø, 2007).

© IEOM Society International

The effect of notches in vortex-induced vibrations has been studied experimentally. Wang et al. studied the effects of rectangular notches on vortex-induced vibrations experimentally (Wang et al., 2023). The study focused more on increasing the amplitude of vortex-induced vibrations as the study focused on energy harvesting applications compared to structural applications.

The effect of the height ratio of triangle groove strips (TGS) on the VIV suppression of marine riser was numerically investigated by Wang et al (Wang et al., 2023). They concluded that the VIV suppression of TGS performs better initially but then deteriorates, with the height ratio of 0.04 showing the best VIV suppression effect. By securing springs and dashpots between the inner and outer pipes of the standard pipe-in-pipe (PIP) system, Nikoo et al. presented a structure-tuned mass damper (TMD) system. Their numerical findings showed that the optimized PIP system can significantly reduce VIV (Matin Nikoo et al., 2018).

Achieving energy harvesting through the resonance of VIV, which is intended to amplify VIV responses, is another application of vortex-induced vibration. Sun et al. Vortex-Induced Vibration for Aquatic Clean Energy (VIVACE) is the name of the application technology that harvests energy from both hydraulic, such as ocean/river and wind for power production technology and augmentation of heat transfer (Sun et al., 2019). The experimental and numerical studies on VIV-based energy harvesting are also proceeding apace. Experimental research by Modir et al. on the impact of mass ratio on the VIV response of a flexibly mounted circular cylinder revealed that peak oscillation amplitude increased with decreasing mass ratio (Modir et al., 2016).

Previous research on notched cylinders predominantly on a single type of notch across a range of geometries. This study addresses that gap by using a numerical approach to conduct a comprehensive comparison of various notched geometries. The goal is to evaluate and contrast the fluid flow and vibration characteristics associated with different notch shapes, providing a more robust understanding of their influence on mechanical behavior.

3. Methodology

3.1 Mathematical Modeling

The study focuses on the comparison of Vortex Induced Vibration (VIV) for 3 different types of notched cylinders (Figure 3) and compares the characteristics of a smooth cylinder. The numerical modeling is done on ANSYS utilizing a two-way FSI (Fluid Structure Interaction) algorithm, which is a transient analysis comprising data transfer between the fluid solver (ANSYS FLUENT) and the structural solver (ANSYS MECHANICAL), and utilizing the Arbitrary Lagrangian-Eulerian (ALE) Approach for mesh refinement in each timestep. The details of the numerical setup are explained in detail in the following sections.

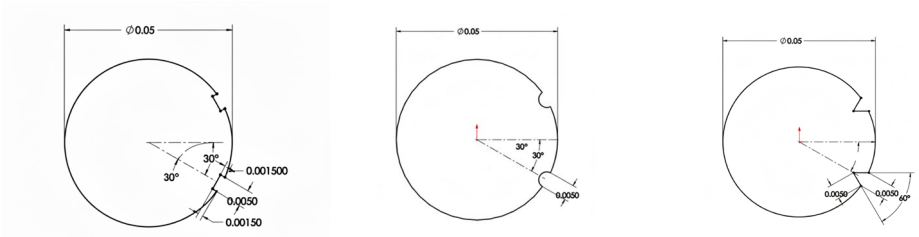

a) Rectangular Notched b) Semicircular Notched c) Triangular Notched

Figure. 3. Cross Sections of different notched cylinders.

Both the solid domain and the fluid domain are simultaneously solved. Therefore, there will be distinct sets of equations that are independently solved for the solid and fluid models.

© IEOM Society International

3.1.1 Governing Equations for Fluid Solver

The first equation, the continuity equation, is an expression representing the concept that matters in a flow that is conserved. Per unit volume, the sum of all incoming and outgoing masses per unit of time must equal the change in mass due to density change per unit of time. The equation can be written in the following way.

$$\frac{\partial \rho}{\partial t} + div(\rho u) = S_m \dots\dots\dots\dots\dots\dots\dots\dots\dots\dots\dots\dots\dots\dots\dots\dots\dots\dots\dots\dots (Eq. 1)$$

Here, where u is the velocity vector with components in the x, y, and z directions, respectively; ρ is the density of the fluid, and t is time; Sm is the amount of mass added to the system. Since the problem is solved in a transient model, the time-dependent factor will be of great importance in this instance (Tu et al., 2024).

The second equation, for the principle of conservation of momentum, is based on the second law of Newton which states that the rate of change of momentum of a particle in a fluid is equal to the sum of the forces acting on the particle. The forces acting on a body consist of both surface forces and body forces. When this law is applied to Newtonian fluids (where viscous stress is proportional to deformation rates), the resulting equations are known as the Navier-Stokes equations. The following equations illustrate the momentum conservation principle (Versteeg & Malalasekera, n.d.).

$$\frac{\partial(\rho u)}{\partial t} + div(\rho u u) = -\frac{\partial p}{\partial x} + div(\mu\, grad\, u) + S_{Mx} \dots\dots\dots\dots\dots\dots\dots (Eq. 2)$$

$$\frac{\partial(\rho v)}{\partial t} + div(\rho v u) = -\frac{\partial p}{\partial y} + div(\mu\, grad\, v) + S_{My} \dots\dots\dots\dots\dots\dots\dots (Eq.\ 3)$$

$$\frac{\partial(\rho w)}{\partial t} + div(\rho w u) = -\frac{\partial p}{\partial z} + div(\mu\, grad\, w) + S_{Mz} \dots\dots\dots\dots\dots\dots\dots (Eq. 4)$$

where ρ is the density, u is the velocity vector *u, u, v,* and *w* are the velocity components in the Cartesian coordinate system, μ is the dynamic viscosity, and S_M is the momentum source term. Since the issue at hand does not involve heat transfer, the energy equation is disregarded.

For solving the equations numerically, the finite volume method was used. In well-established commercial CFD codes, the finite volume method is one of the numerical techniques used to solve the governing equations of the fluid. Fluent employs the finite volume technique to transform the general transport equation into a system of algebraic equations and then employs various iterative methods to solve the algebraic equations. The following are the essential steps for solving the transport equation for a physical quantity (Versteeg & Malalasekera, n.d.). The general form of the transport equation can be expressed in conservative form as shown below.

$$\frac{\partial(\rho\phi)}{\partial t} + \mathrm{div}(\rho\phi \mathrm{u}) = \mathrm{div}(\Gamma\, \mathrm{grad}\, \phi) + S_\phi \dots\dots\dots\dots\dots\dots\dots\dots\dots\dots\dots\dots (Eq.\ 5)$$

Here, φ can be replaced by any scalar quantity, and the diffusion coefficient is denoted by Γ. The following equation is obtained by integrating over the control volume and applying Gauss's divergence theorem to the general transport equation.

$$\frac{\partial}{\partial t}\int_{CV} \rho\phi dV + \int_A n(\rho\phi \mathrm{u}) dA = \int_A n(\Gamma \mathrm{grad}\ \phi) dA + \int_{CV} S_\phi dV \ \dots\dots\dots (Eq.\ 6)$$

For turbulence modeling the Shear-Stress Transport (SST) *k-**ω*** Model was used.

3.1.2 Governing Equations for Structural Solver

For transient dynamic analysis, impulse loads are a type of dynamic load that acts on large structures within a short time interval. For calculating the time history analysis of the loaded structure, the basic equation of motion for the system is given as follows:

$$m\ddot{u} + c\dot{u} + ku = p(t) \dots\dots\dots\dots\dots\dots\dots (Eq.\ 7)$$

Here m is the structural mass matrix, $\ddot{u}$ is an acceleration vector, *c* is a structural damping matrix, $\dot{u}$ is a velocity vector, *k* is a structural stiffness matrix, *u* is a displacement vector, and *p* is a force vector, which is a function of time.

In the current model, the equation used is

© IEOM Society International

$$m\ddot{u}+ku = p(t) \ldots \ldots \ldots \ldots \ldots \text{(Eq. 8)}$$

The damping term is zero in this instance because no structural damping is used in most linear structural problems.

3.2 Geometry and Mesh

3.2.1 CFD Domain

Using ANSYS 2020 R1's Design Modeler design software, the model's domains were developed. The fluid domain is constructed as a square prism with a cylindrical element. Following is a diagram of the full fluid domain with dimensions, followed by a diagram of the structural member fixed to the symmetrical walls of the fluid domain.

Hexahedral elements are utilized to construct the surface mesh, which is then used to create the volume mesh, in the case of the CFD mesh. The volume of mesh falls under the structured mesh category. In a CFD model, boundary layers typically call for special consideration. The y^+ value (non-dimensional distance from the wall to the first cell) is regarded as a crucial parameter in this treatment. The turbulence model's wall functions, which deal with the flow in the boundary layer, have some limitations on the y^+ values at the wall. Keep the standard y^+ value below 1. The initial layer thickness for this mesh is maintained so that the y^+ value is 0.9. Edge sizing and biasing are applied in ANSYS meshing to achieve this.

The optimum mesh size was chosen after the mesh independence test. The mesh independence test was conducted at a 10,000 Reynolds number for a steady state condition. The total fluid domain was divided into 12 different zones for the ease of application of the grid size and for creating a uniform structured mesh. Biasing was used, and the bias factors were changed for zones where rapid changes in flow characteristics were observed. The grid divisions were changed for each step of the mesh independence test. In the end, the mesh was tested for 314550 to 1620550 number of elements. The result of the mesh independence test can be seen below. It can be seen that there is only a change of 0.08% in the value of C_d between the last two iterations of the mesh independence test (Table 1, Figure 4).

Table 1. Table for mesh independence test of the model

Number of Elements	Coefficient of Drag
314550	7.35E-01
334350	7.40E-01
412350	7.45E-01
512350	7.48E-01
714750	7.54E-01
1013750	7.64E-01
1311750	7.64E-01
1620550	7.64E-01

© IEOM Society International

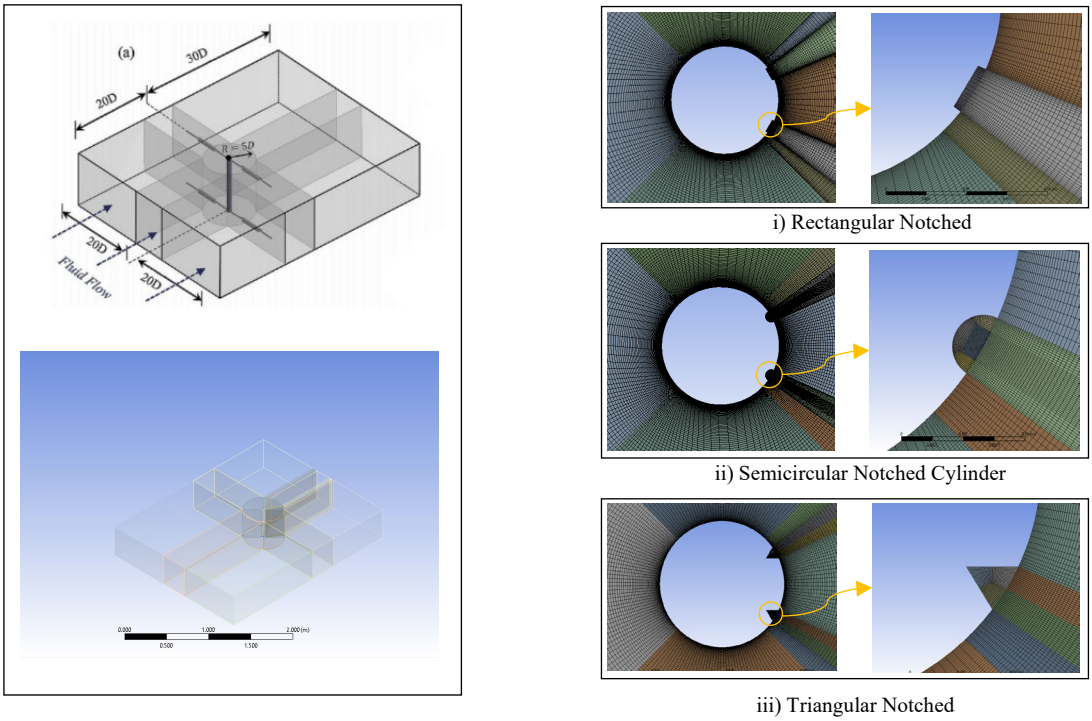

Figure 4. a) CFD domain and mesh topology for all cylinders; b) CFD mesh closeup for different notched cylinders.

3.2.2 CSM Domain

Hexahedron meshing is the most prevalent type of meshing in 3D modeling. Mesh quality is crucial to achieving the most precise results. ANSYS Mesh implementation uses meshing. The 3D model is used to produce a structured hexahedral mesh for simulation.

The solid domain was divided into five different parts for the application of the sizing function during the meshing of the solid domain. This allowed for a uniform, structured mesh to be obtained on the solid element. The CSM mesh grid sizes were chosen in such a way that they corresponded to the nodes in the fluid solver, FLUENT. This is done to permit force transfer during the coupling iterations in fluid-solid coupling. The corresponding meshes are shown in Figure 5.

© IEOM Society International

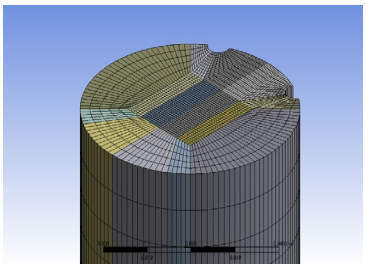

a) Rectangular Notched

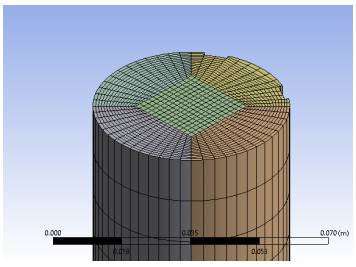

b) Semicircular Notched

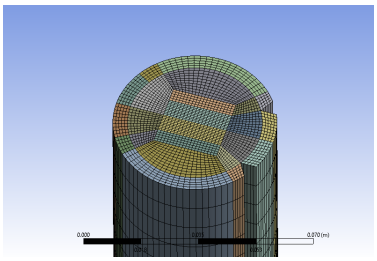

c) Triangular Notched

Figure 5. CSM mesh topology for all cylinders

3.3 Computational Setup

3.3.1 Computational Setup for Fluid Solver

In this present study, the numerical problem is solved using a pressure-based solver by ANSYS Fluent. The fluid used was atmospheric air. The fluid properties are discussed below in Table 2.

Table 2. Material Properties for the fluid solver

Parameter	**Value**
Density	1.225 kg/m^3
Dynamic viscosity	1.7894*10^{-05} kg/m.s
Reynolds number	10,000

The various settings for the setup are mentioned below in Table 3 – Table 7.

Table 3. Solution settings for the fluid solver

Parameter	**Setup/Value**
Solver Type	Pressure-Based
Velocity Formulation	Absolute
Time	Transient
Multiphase	Off
Viscous Model	Turbulent (SST k-ω) with low-Re correction
Radiation	Off
Fluid	Air

© IEOM Society International

Table 4. Solution methods for the fluid solver

Settings	Selection
Temporal discretization	2nd order
Turbulence model	k-ω and SST models
Pressure	Standard
Pressure-velocity coupling	SIMPLE
Gradient	Least Square Based
Momentum	2nd order upwind
Turbulent Kinetic energy	2nd order upwind
Turbulent dissipation rate (for k-ω model)	2nd order upwind
Specific dissipation rate (for SST model)	2nd order upwind
Transient Formulation	2nd order implicit

Table 5. Solution controls for the fluid solver

Parameter	**Setup/Value**
Pressure	0.3
Density	1
Body Forces	1
Momentum	0.7
Turbulent Kinetic Energy	0.8
Specific Dissipation	0.8
Turbulent Viscosity	1

The boundary conditions are shown in Figure 6.

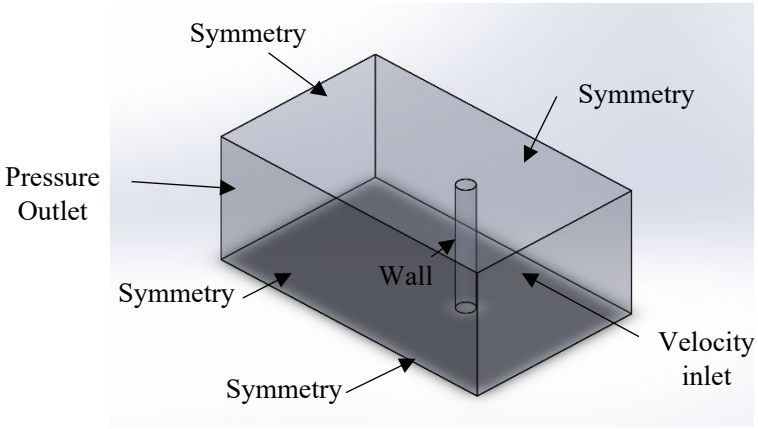

Figure 6. Boundary conditions for the fluid solver.

© IEOM Society International

Table 6. Boundary conditions for the fluid solver

Inlet	Velocity Inlet
Outlet	Pressure Outlet
Top Wall	Symmetry
Bottom Wall	Symmetry
Side Walls	Symmetry
Cylinder Wall	No slip, wall

3.3.2 Computational Setup for Structural Solver

Another set of boundary conditions is applied to the solid solver, ANSYS Mechanical, separately. The boundary conditions for the solid solver are shown in Figure.7.

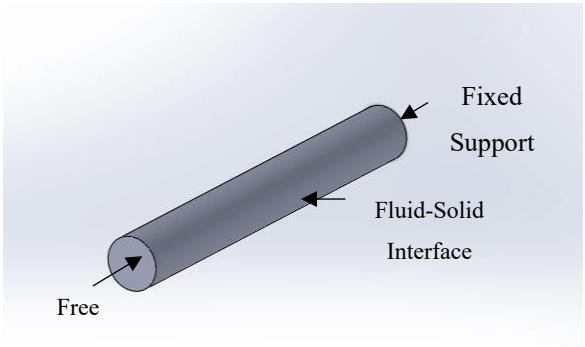

Figure 7. Boundary conditions for the solid solver.

Table 7. Material properties of the solid solver

Parameter	Value
Density	7800 kgm-3
Poison's Ratio	0.3
Young's Modulus	200,000 MPa

Auto time stepping was turned off so that the system coupling module could control the time step of Fluent and ANSYS Mechanical simultaneously. Step control was defined by substeps for the same purpose.

3.3.3 Computational Setup for Fluid Structure Interaction (FSI)

System Coupling was achieved using ANSYS Workbench's system coupling module. Workbench's system coupling tool integrates many domain solvers into multi-physics simulations. The FSI analysis setup for this project's work is shown in the above Figureure using System coupling and the numerical solvers Fluent and ANSYS Mechanical. The setup components of the solvers are then merged into the setup component of System Coupling, as seen after running the simulation setups for both solvers in the earlier sections. As a result, the System Coupling can now recognize the contact between the fluid and the structure and synchronize the numerical conditions of both solvers. The timestep size was determined using Courant-Friedrichs-Lewy (CFL), which states that the timestep size should be less than or equal to the minimum time it takes for a disturbance to travel across one computational cell. This condition ensures

© IEOM Society International

that the numerical scheme is stable and accurate, and it can be used to estimate the maximum timestep size based on the grid size and the local velocity of the flow.

$$C = u\frac{\Delta t}{\Delta x} \dots\dots\dots\dots\dots\dots\dots\dots\dots (Eq. 9)$$

(Eq. 9) C represents the courant number. And Δt and Δx are the timestep size and average mesh size respectively. Ideally, the timestep size has to be kept low enough so that the courant number is below 0.7. However, the CFL condition is only a necessary condition for stability, and it may not always be sufficient to guarantee accurate results. Other factors such as the viscosity of the fluid, the presence of shocks or turbulence, and the accuracy of the numerical scheme can also affect the choice of timestep size. To select an appropriate timestep size, the user must first estimate the characteristic timescale of the problem being simulated. This timescale can be related to the geometry of the simulation domain, the flow velocity, and other relevant parameters. Once the characteristic timescale is known, the timestep size should be chosen such that it is smaller than this timescale.

For the CFD mesh, timescales between 0.08 and 0.00125 were simulated. For simulating each timestep size, the chosen timestep was half of the previously chosen timestep. From the following Table 8, the difference in the value of C_{dmean} for the last two timesteps is only 0.96%, which is within acceptable limits.

Table 8. Timestep independence test for the model

Timestep Size (s)	Mean coefficient of Drag
0.08	1.73736
0.04	1.43256
0.02	1.42875
0.01	1.41478
0.005	1.42605
0.0025	1.41109
0.00125	1.42467

4. Results

4.1 Comparison of Velocity Contours for Different Models

The vortex generation phenomenon can be observed directly through velocity contours. Observing Figure. 8- Figure 14 it is seen that during the initial stages of flow development, the flow separation is almost symmetrical for the smooth cylinder as well as cylinders with notched geometries.

© IEOM Society International

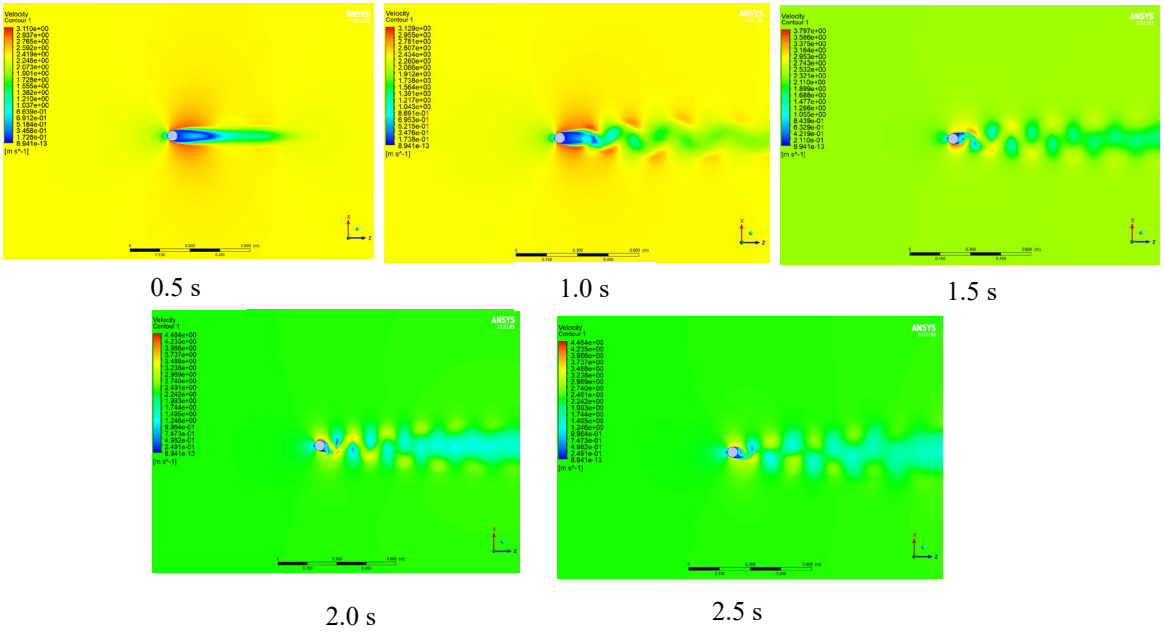

Figure 8. Velocity contours for smooth cylinder.

But as the flow becomes more developed, the characteristics in the wake region are more asymmetrical. The flow readily separates and created regions of high and low velocities, and resulting vortices are also created. The flow rushed past the cylinder, creating vortices behind it. The vortex shedding was clearly visible in each of those images and it was therefore possible to draw the conclusion that the vortex shedding was associated with velocity magnitude.

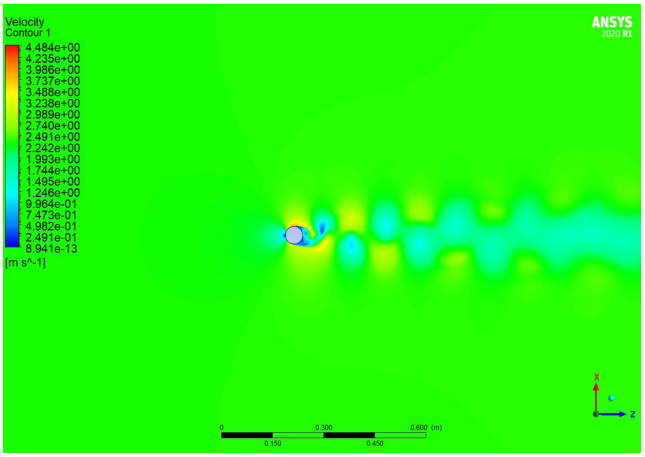

Figure 9. Velocity contour for smooth cylinder for fully developed flow (3.0 s).

© IEOM Society International

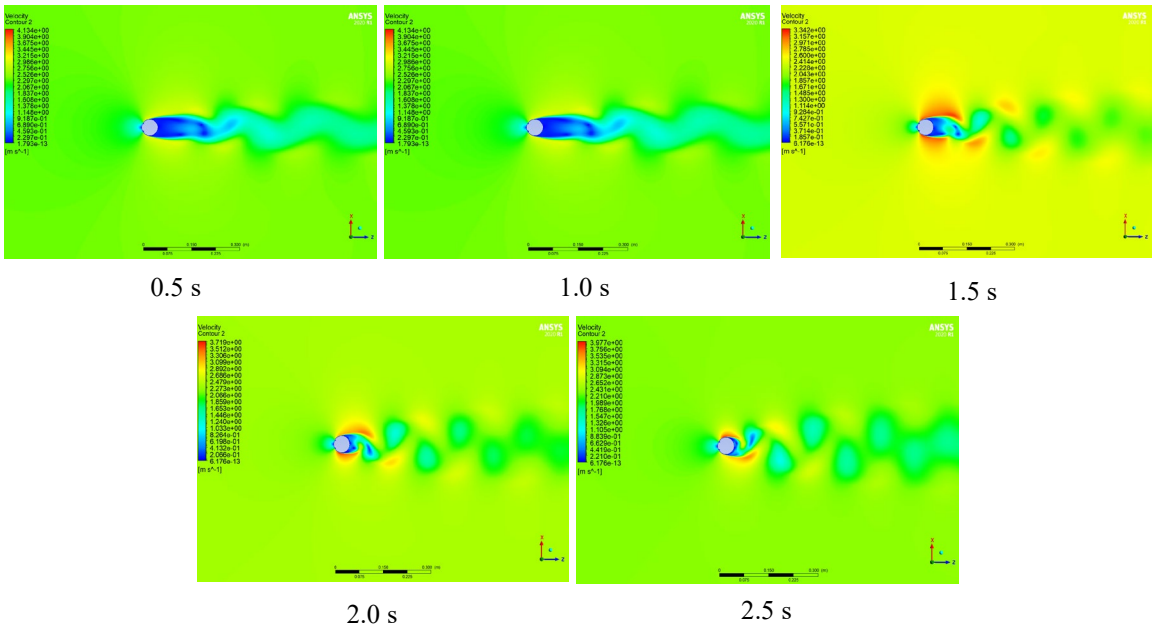

Figure 10. Velocity contours for cylinder with triangular notches.

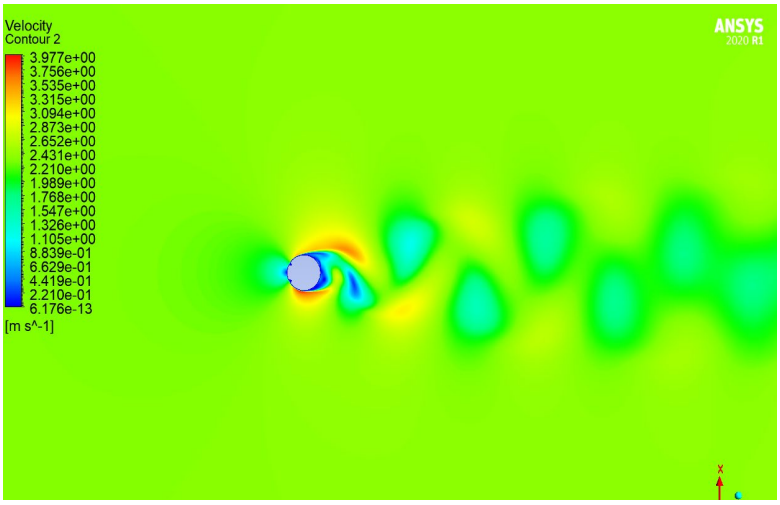

Figure 11. Velocity contour for cylinder with triangular notches for fully developed flow (3.0 s).

© IEOM Society International

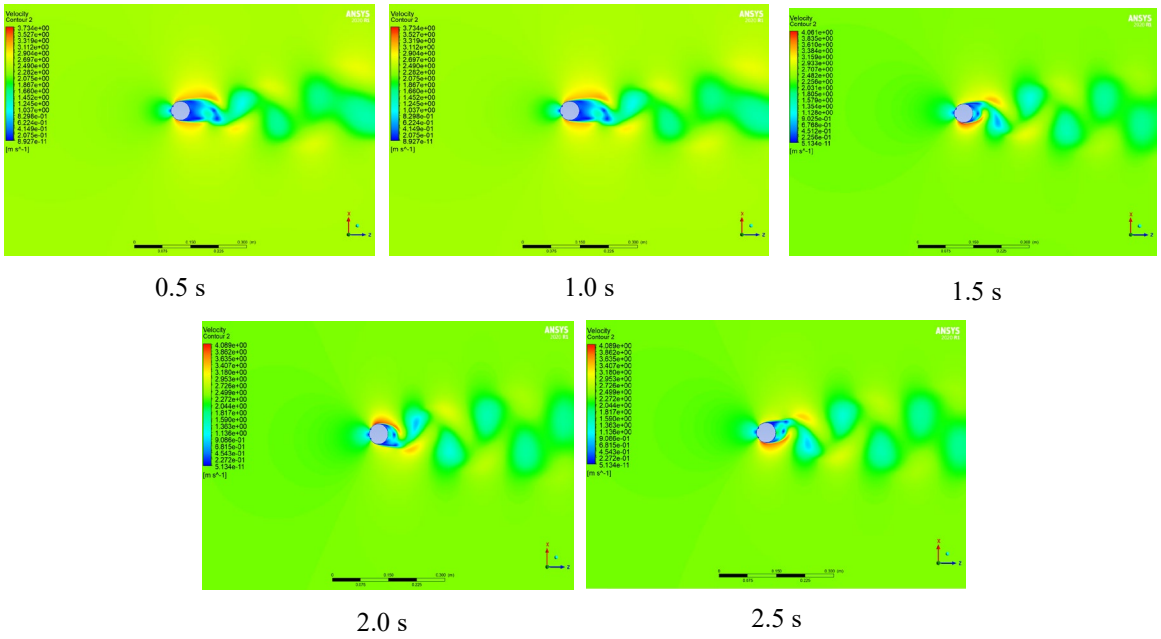

Figure 12: Velocity contours for cylinder with semicircular notches.

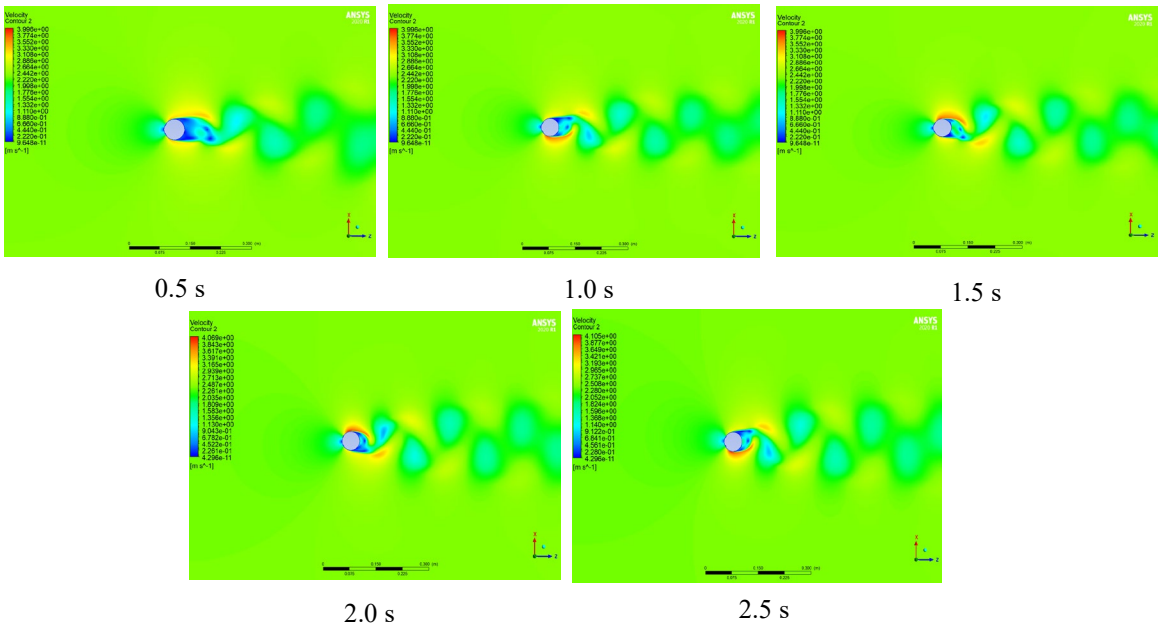

Figure 13. Velocity contours for cylinder with rectangular notches.

© IEOM Society International

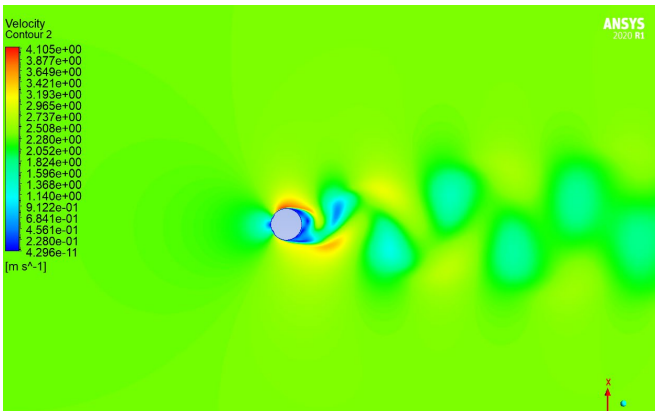

Figure 14. Velocity contour for cylinder with rectangular notches for fully developed flow (3.0 s).

Comparing the contours of velocity for fully developed flow, it is seen that in the case of triangular notched cylinder, flow separation occurs relatively fast compared to others. For this phenomenon, the corresponding forces in the direction perpendicular to the flow direction will also be much higher, which in return will result in more deformation of the vibrating body. The vortex shedding mode can be identified from the velocity contours. It can be seen that all types of geometries shed vortices at 2S mode.

4.2 Comparison of Turbulent Kinetic Energy Contours for Different Geometries

The effect of turbulent kinetic energy can be seen in Figure. 15- Figure 22. Turbulent kinetic energy is related to the behavior of vortices and shear layers in a fluid flow. In regions of high vorticity and shear, the TKE is typically high, indicating that the flow is highly turbulent and energetic. The contours in the following Figureures indicate discrete regions of high turbulent energy, which indicate the vortices being generated in the wake region of the flow. The results correlate with the findings from the velocity contours.

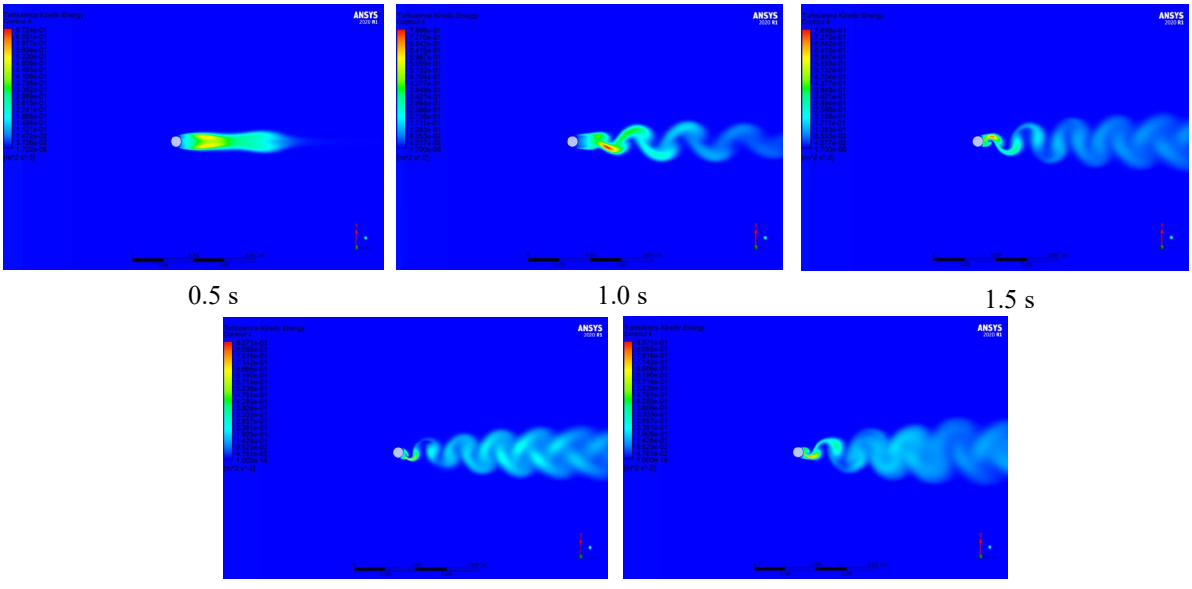

Figure 15. Turbulent Kinetic Energy contours for smooth cylinder.

© IEOM Society International

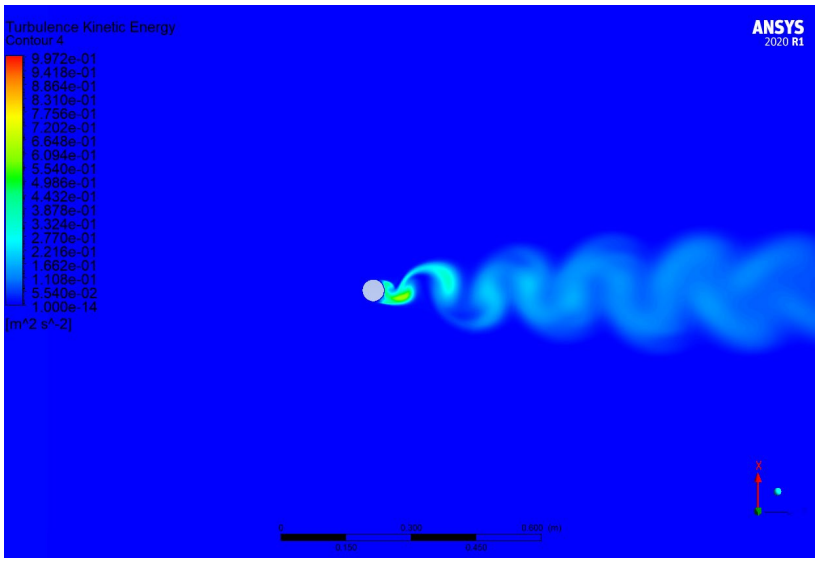

Figure 16. Turbulent kinetic energy contour for smooth cylinder for fully developed flow (3.0 s).

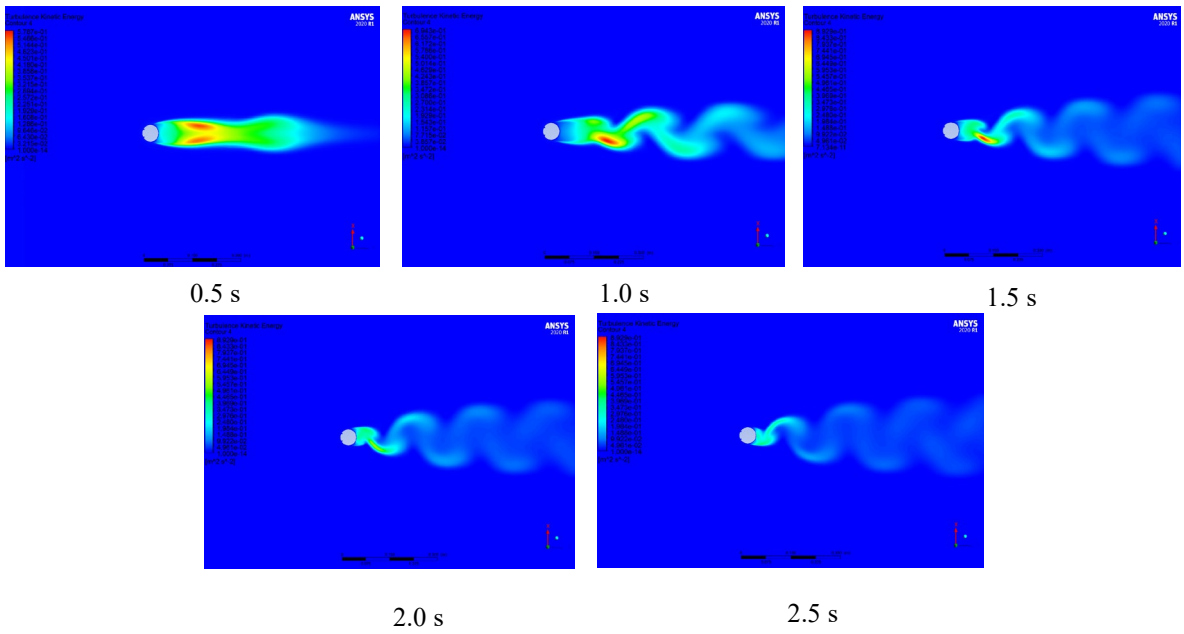

Figure 17. Turbulent Kinetic Energy contours for cylinder with triangular notches.

© IEOM Society International

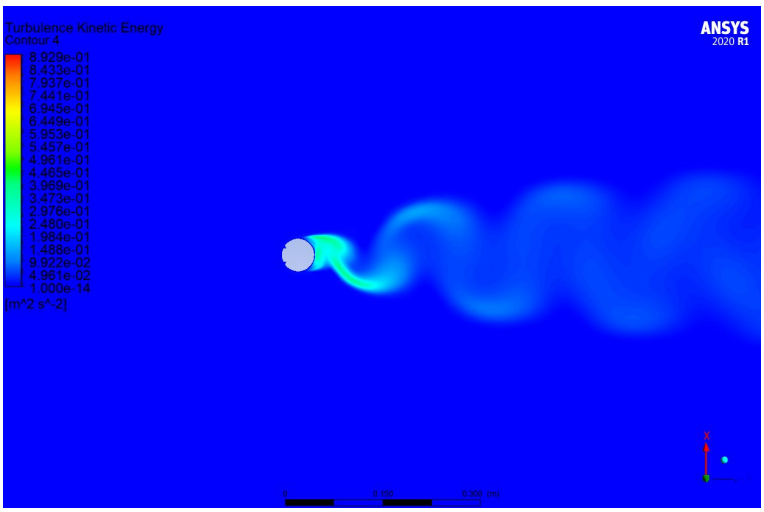

Figure 18. Turbulent Kinetic Energy contour for cylinder with triangular notches for fully developed flow (3.0 s).

The triangular notch, with its acute-angle discontinuity, generates the most distinct separation, leading to the formation of vortices with higher circulation. This indicates the generation of higher body forces and resulting deformation in the cylinder. Further discussion of body forces is in the following sections.

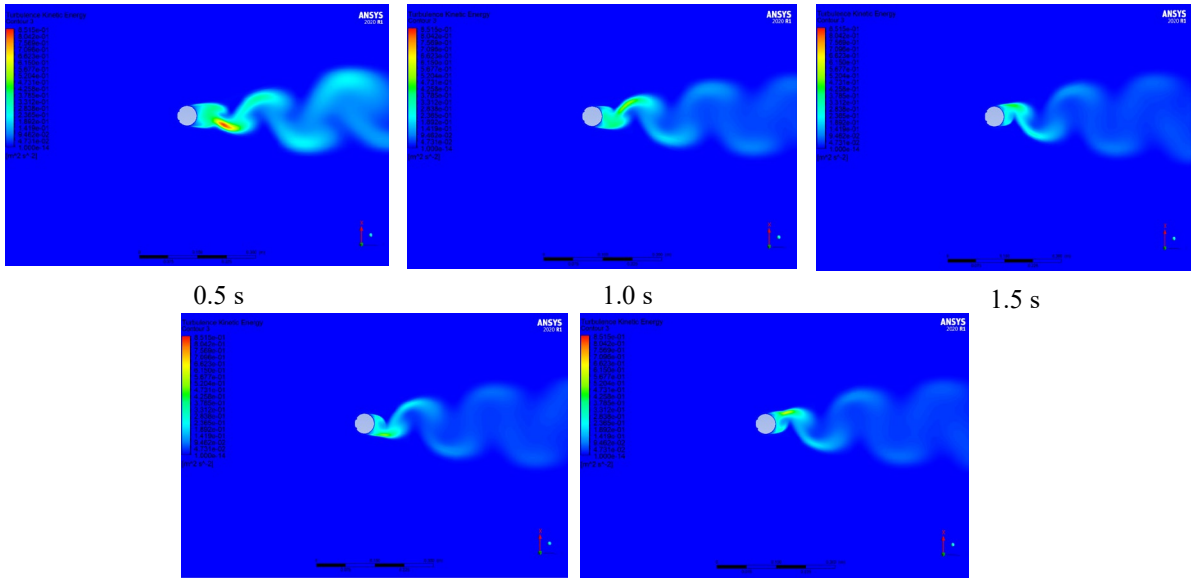

Figure 19. Turbulent Kinetic Energy contours for cylinder with semicircular notches.

© IEOM Society International

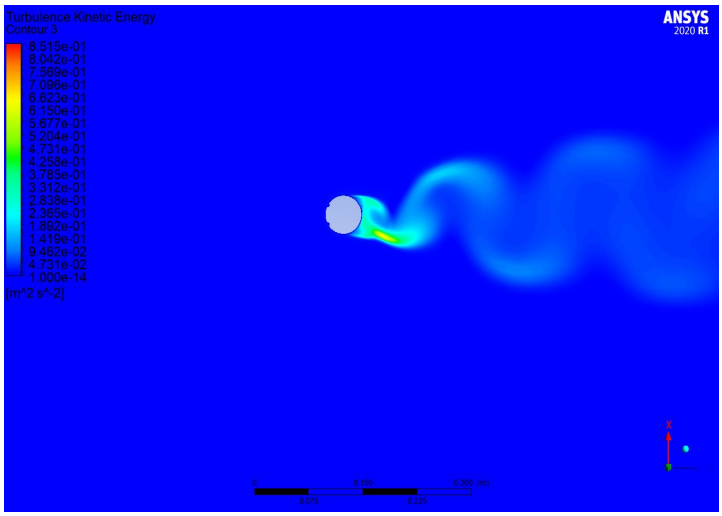

Figure 20. Turbulent Kinetic Energy contour for cylinder with semicircular notches for fully developed flow (3.0 s).

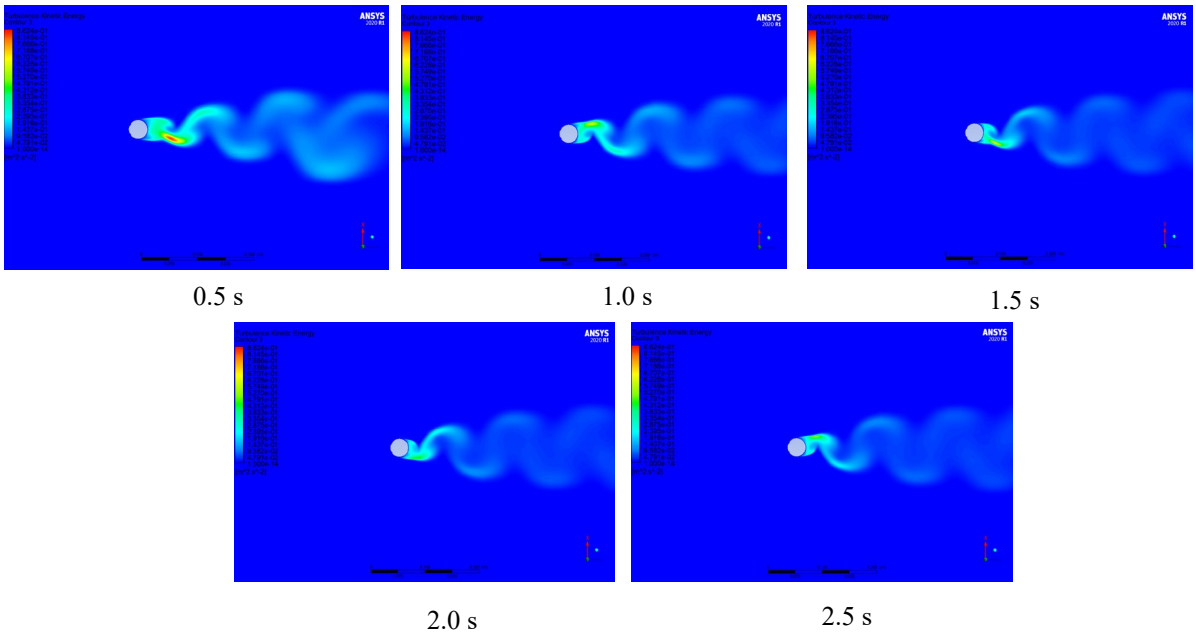

Figure 21. Turbulent Kinetic Energy contours for cylinder with rectangular notches.

© IEOM Society International

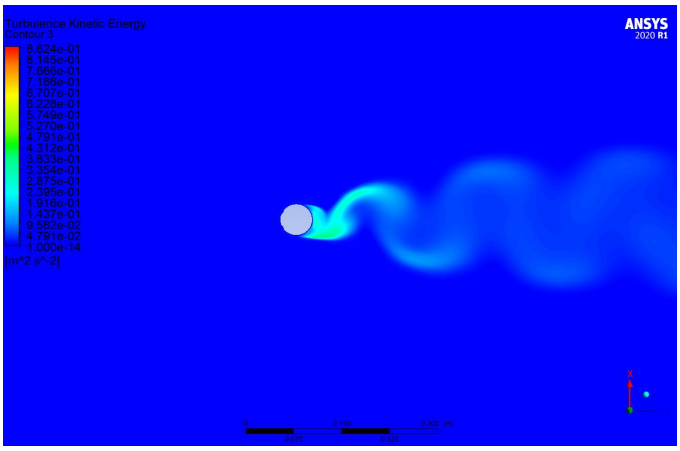

Figure 22. Turbulent Kinetic Energy contour for cylinder with rectangular notches for fully developed flow (3.0 s).

The effect of notch geometry on the VIV response is mainly due to changes in the way the boundary layer separates. The sharp edges of the notches act as fixed geometric triggers, making the boundary layer detach suddenly. This is different from a smooth cylinder, where the separation point moves around. This forced separation makes the shear layers stronger, which raises the Turbulent Kinetic Energy (TKE) in the near-wake region. This is shown by the high-intensity areas in the TKE contours for all notched cylinders. A lot of momentum is being exchanged in the shear layer when the TKE is high. This makes it easier for fluids to get in quickly and speeds up the process of rolling up the vortex. This higher level of turbulent energy makes the shedding vortices stronger, which directly leads to the stronger hydrodynamic forces that are seen.

4.3 Comparison of Vorticity Generation for Different Geometries

Shedding of vortices can be easily identified in the vorticity contours in Figure 23. By magnitude, the rectangular notched geometry has the highest amount of vorticity, specifically around the sharp edges of the notch. All the notched cylinders generate higher peak local vorticity at their sharp edges; this high local vorticity has the potential to work as a flow stabilization mechanism, consequently stabilizing the body forces on the cylinders.

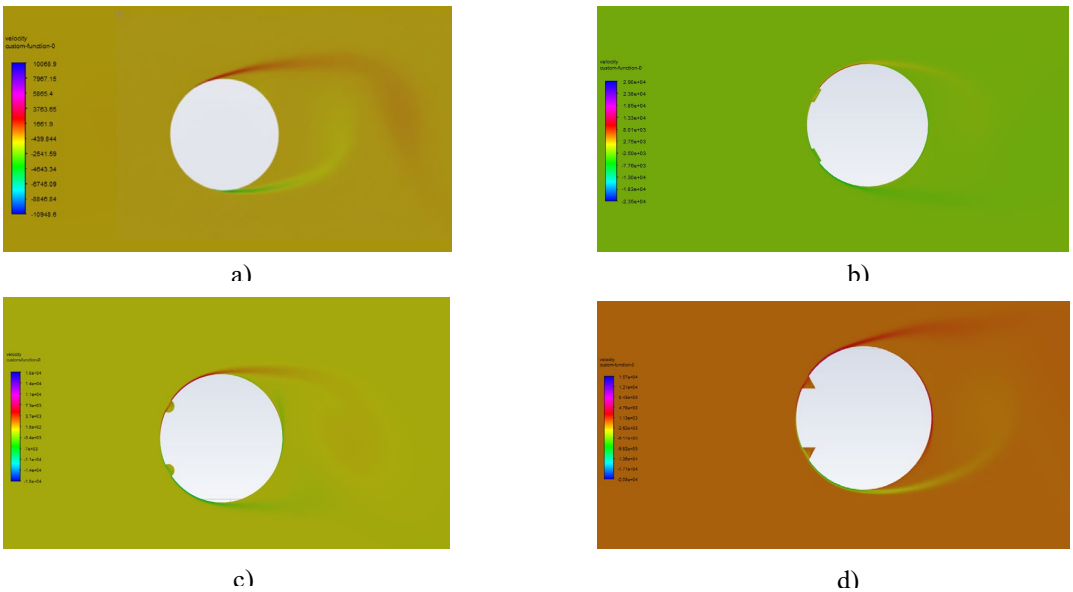

Figure 23. Vorticity contours for fully developed flow around different cylinders. a) Smooth Cylinder; b) Rectangular Notched Cylinder; c) Semicircular Notched Cylinder; d) Triangular Notched Cylinder.

© IEOM Society International

4.4 Comparison of Body Forces and Deformations for Different Geometries

Comparing the different notched geometries among notched geometries, flow develops more rapidly in the case of rectangular notched geometry, followed by semicircular notched geometry. From Figure 24 it can be observed that flow takes the most time for the triangular notched geometry model, comparatively. But the maximum body force is observed for the cylinder with triangular notches.

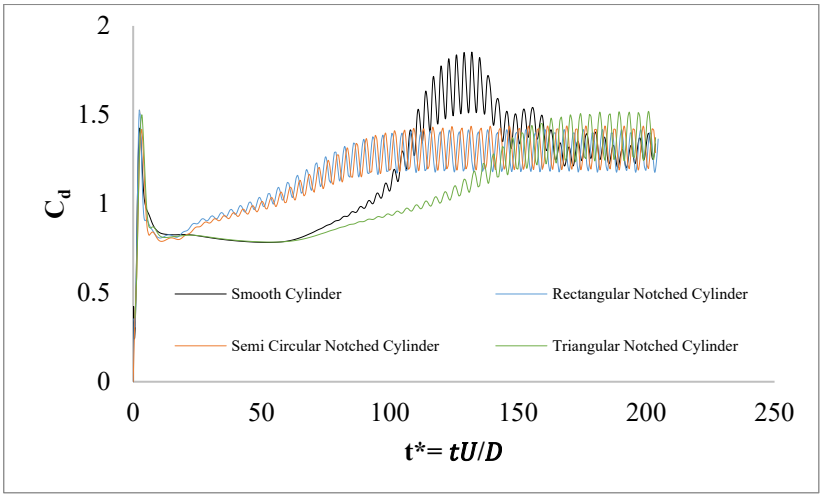

Figure 24. Comparison of the Coefficient of drag over varying time for different cylinder geometries.

As shown in Table 9, the triangular notched cylinder exhibited the highest mean drag Cd_{mean} = 1.36 representing a 15.3% increase over the smooth profile. The semicircular Cd_{mean} = 1.32 and rectangular Cd_{mean} = 1.29 notches also demonstrated elevated drag values. This increase is attributed to the surface discontinuities disrupting the boundary layer attachment, leading to earlier flow separation and a wider, more turbulent wake region. While this increased drag imposes a higher structural load, it further confirms that the triangular notch induces the most significant hydrodynamic disturbance among the tested geometries. All the mean values were taken for the fully developed flow region.

Table 9. Comparison of Cd_{mean}

Geometry Type	**Cd_{mean}**
Smooth Cylinder	1.18
Rectangular Notched Cylinder	1.29
Semicircular Notched Cylinder	1.32
Triangular Notched Cylinder	1.36

The influence of notch geometry on the hydrodynamic forces was quantified by analyzing the root-mean-square lift coefficient Cl_{rms} for each cylinder for fully developed flow (Figure 25- Figure 27).

© IEOM Society International

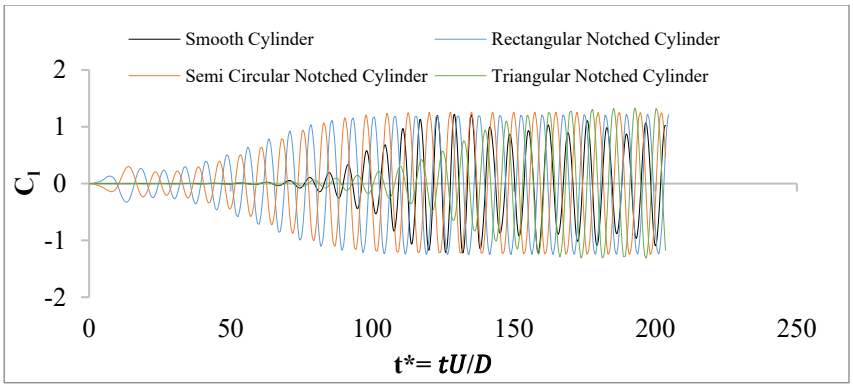

Figure.25. Comparison of the coefficient of lift over varying time for different cylinder geometries.

As detailed in Table 10, the presence of surface notches consistently augmented the fluctuating lift forces compared to the smooth cylinder baseline C_{lrms} = 0.66. The triangular notched cylinder exhibited the most pronounced response, reaching a C_{lrms} = 0.93, which represents a 40.9% increase in lift magnitude over the smooth cylinder. The semicircular C_{lrms} = 0.87and rectangular C_{lrms} = 0.83 geometries followed (Table 10), indicating that while all notches destabilize the flow field to enhance vortex strength, the sharp, angled discontinuity of the triangular notch is most effective at intensifying the cross-flow forces. This significant amplification in lift force directly correlates with the maximum structural deformation observed in the triangular geometry, confirming that the increased vibration amplitude is driven by stronger vortex-structure energy transfer.

Table 10. Comparison of Cl_{rms}

Geometry Type	**Cl_{rms}**
Smooth Cylinder	0.66
Rectangular Notched Cylinder	0.83
Semicircular Notched Cylinder	0.87
Triangular Notched Cylinder	0.93

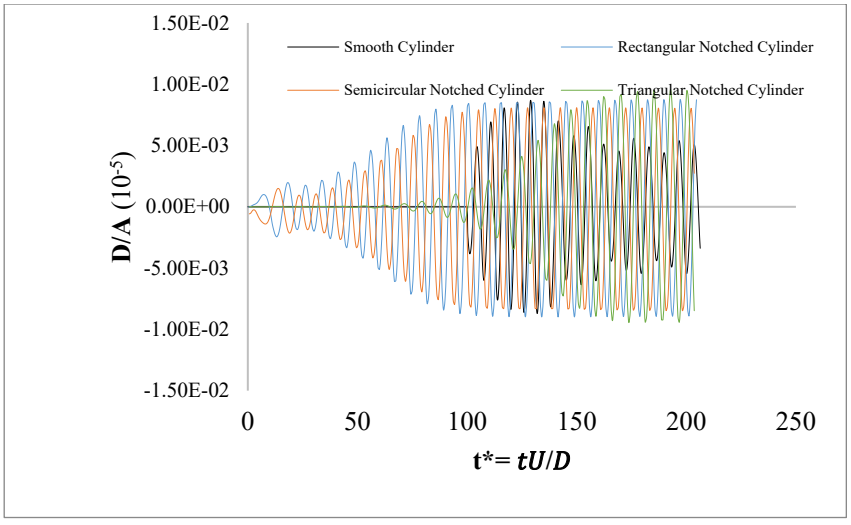

Figure 26. Comparison of the deformation over varying time for different cylinder geometries.

The deformation of the cylinder bodies can be seen in Table 11. follows the same pattern as the lift forces on the body, as lift forces are the only force causing lateral deformation. Compared to the smooth cylinder, triangular notches show the highest (20.80%) increase in deformation, followed by semicircular notches (14.98%) and rectangular notches.

© IEOM Society International

Table 11. Comparison of Deformation

Geometry Type	$(d/A)_{max}$(E-08)	Percentage of Deviation
Smooth Cylinder	7.98	0
Rectangular Notched Cylinder	8.74	10.65
Semicircular Notched Cylinder	9.086	14.98
Triangular Notched Cylinder	9.55	20.80

4.5 Comparison of Strouhal Number for Different Geometries

A Fast Fourier Transform was done on the lift forces. From the plotted graphs for the Strouhal number, it can be seen in Table 7 that the value of the Strouhal number is closest to 0.2 for triangular notched geometry and the farthest for the smooth cylinder. This data is compliant with previous observations. So, now it can be concluded that the flow is the most stable for the triangular notched geometry and the least stable for the smooth cylinder.

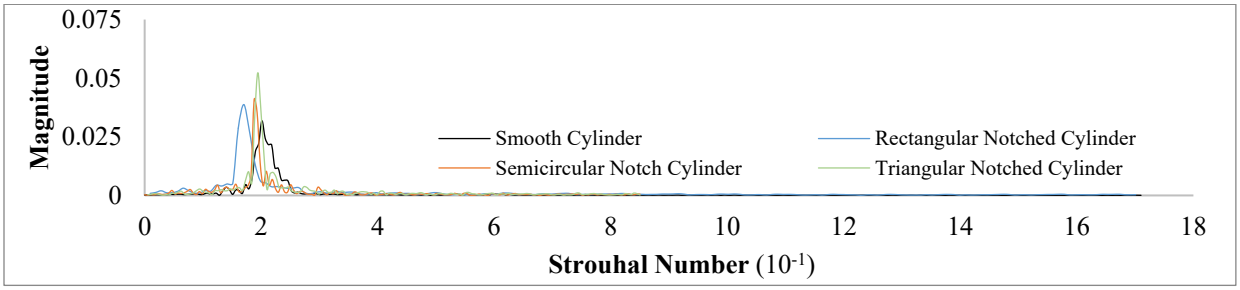

Figure 27. Comparison of Strouhal Number for different cylinder geometries.

The vortex-shedding frequencies can be calculated from the Strouhal numbers for all models. Since vortex shedding frequency is proportional to the Strouhal number, similar trends in values are seen.

Table 12. Comparison of Strouhal number and vortex shedding frequency

Geometry Type	St	f_s
Smooth Cylinder	0.180	8.617285
Rectangular Notched Cylinder	0.183	8.760907
Semicircular Notched Cylinder	0.188	9.000276
Triangular Notched Cylinder	0.194	9.287519

The Strouhal number (St) is the main way to tell how often and how well the vortex street is organized. In the subcritical Reynolds number range, a Strouhal number of about 0.2 is typical of a von Kármán vortex street that is fully developed and stable. The triangular notched cylinder has a Strouhal number of 0.1942, which is the closest to the theoretical ideal value of 0.2, as shown in Table 12. This wake stability, which is the regularity of vortex formation, is very important for VIV amplification. A very regular wake makes sure that energy is transferred from the fluid to the structure in a consistent and synchronized way. This is what causes the amplified deformation seen in the triangular shape. On the other hand, deviations that are far from 0.2 would mean that the shedding frequency is disorganized or happens at random times, which is not as good at keeping high-amplitude structural oscillations going.

5. Limitations

While this study provides a robust two-way FSI analysis, certain limitations exist. First, the simulation was conducted at a single Reynolds number (Re=10,000), limiting the generalization of results across different flow and vibration regimes. Secondly, the study utilized a RANS-based turbulence model (k-ω SST), which, while computationally efficient, averages the finest turbulent scales that a Large Eddy Simulation (LES) would capture.

6. Conclusion

After carrying out the numerical investigation of vortex-induced vibration (VIV) in notched circular cylinders a two-way FSI framework we can conclude that triangular notches generate the strongest VIV response, with up to 20.8%

© IEOM Society International

higher deformation compared to a smooth cylinder, while rectangular and semicircular notches promote relatively stable vortex shedding. These findings highlight the influence of notch geometry on VIV characteristics and provide design-level insights for cylindrical structures exposed to cross-flow. Future work will consider a broader range of Reynolds numbers with variations in the notch geometry and experimental validation.

7. Future Work

Based on the findings of this study, the following recommendations can be made for future research:

I) **Investigation of the effect of different notch geometries on VIV behavior for different flow regimes:** This study focused on fluid flow over a circular cylinder at only one flow regime, but different flow regimes, such as laminar flow, may lead to different VIV behavior. Future research can explore the effects of different notch geometries on VIV behavior for a range of flow regimes.

II) **Consideration of the effect of notches on fatigue life:** While this study focused on the VIV response of a structure, notches may also affect the fatigue life of a structure. Future research can investigate the effect of notches on fatigue life and how this affects the design of structures exposed to fluid flow for different materials.

III) **Optimization of the design of notches for specific applications:** The findings of this study suggest that the geometry of notches plays a critical role in determining the VIV response of a structure. Future research can explore the optimal notch designs for specific engineering applications such as minimizing the risk of VIV-induced damage or increasing VIV for energy harvesting applications.

Acknowledgements

The authors would like to express gratitude to the Department of Mechanical Engineering, KUET, for supporting this project. The authors would like to convey their most sincere gratitude to Prof. Dr. Zahir Uddin Ahmed, Professor, Department of Mechanical Engineering, Khulna University of Engineering & Technology, Khulna, for providing valuable guidance and support.

Funding Statement

This project did not receive any external financial support; it was fully funded by the authors.

References

Amabili, M., Review of The theory and practice of hydrodynamics and vibration by S. K. Chakrabarti, Journal of Sound and Vibration, vol. 270, no. 4–5, p. 1091, 2004.

Argyropoulos, C. D., and Markatos, N. C., Recent advances on the numerical modelling of turbulent flows, Applied Mathematical Modelling, vol. 39, no. 2, pp. 693–732, 2015.

Bearman, P. W., Vortex shedding from oscillating bluff bodies, Annual Review of Fluid Mechanics, vol. 16, no. 1, pp. 195–222, 1984.

Behara, S., and Sotiropoulos, F., Vortex-induced vibrations of an elastically mounted sphere: The effects of Reynolds number and reduced velocity, Journal of Fluids and Structures, vol. 66, pp. 54–68, 2016.

Chen, S. S., Flow-induced vibration of circular cylindrical structures, Hemisphere Publishing Corporation, 1987.

Hussein, N., and Baz, A., Active control of vortex-induced vibrations using a continuous sliding mode control, in Proc. AIAA Guidance, Navigation and Control Conf., Aug. 2008.

Islam, S. U., Manzoor, R., and Zhou, C. Y., Effect of Reynolds numbers on flow past a square cylinder in presence of multiple control cylinders at various gap spacings, Arabian Journal for Science and Engineering, vol. 42, no. 3, pp. 1049–1064, 2017.

Islam, S. U., Zhou, C. Y., Shah, A., and Xie, P., Numerical simulation of flow past rectangular cylinders with different aspect ratios using the incompressible lattice Boltzmann method, Journal of Mechanical Science and Technology, vol. 26, no. 4, pp. 1027–1041, 2012.

Khan, N. B., Jameel, M., Badry, A. B. M., and Ibrahim, Z. B., Numerical study of flow around a smooth circular cylinder at Reynolds number 3900 with large eddy simulation, in Proc. ASME OMAE Conf., 2016.

Liangjie, M., Qingyou, L., and Shouwei, Z., Experimental study of the vortex-induced vibration of drilling risers under shear flow with different Reynolds numbers, PLoS ONE, vol. 9, no. 8, p. e104806, 2014.

Matin Nikoo, H., Bi, K., and Hao, H., Effectiveness of using pipe-in-pipe concept to reduce vortex-induced vibrations: A three-dimensional two-way FSI analysis, Ocean Engineering, vol. 148, pp. 263–276, 2018.

© IEOM Society International

Matsumoto, M., Yagi, T., Shigemura, Y., and Tsushima, D., Vortex-induced cable vibration of cable-stayed bridges at high reduced wind velocity, Journal of Wind Engineering and Industrial Aerodynamics, vol. 89, no. 7–8, pp. 633–647, 2001.

Modir, A., Kahrom, M., and Farshidianfar, A., Mass ratio effect on vortex-induced vibration of a flexibly mounted circular cylinder: An experimental study, International Journal of Marine Energy, vol. 16, pp. 1–11, 2016.

Okajima, A., and Kiwata, T., Flow-induced stream-wise vibration of circular cylinders, Journal of Flow Control, Measurement & Visualization, vol. 7, no. 3, pp. 133–151, 2019.

Parkinson, G., Phenomena and modelling of flow-induced vibrations of bluff bodies, Progress in Aerospace Sciences, vol. 26, no. 2, pp. 169–224, 1989.

Placzek, A., Sigrist, J.-F., and Hamdouni, A., Numerical simulation of an oscillating cylinder in a cross-flow at low Reynolds number: Forced and free oscillations, Computers & Fluids, vol. 38, no. 1, pp. 80–100, 2009.

Sun, W., Zhao, D., Tan, T., Yan, Z., Guo, P., and Luo, X., Low velocity water flow energy harvesting using vortex-induced vibration and galloping, Applied Energy, vol. 251, p. 113392, 2019.

Tu, J., Yeoh, G. H., Liu, C., and Tao, Y., Governing equations for CFD – fundamentals, in Computational Fluid Dynamics, Elsevier, pp. 63–122, 2024.

Tutar, M., and Holdø, A. E., Large eddy simulation of a smooth circular cylinder oscillating normal to a uniform flow, Journal of Fluids Engineering, vol. 122, no. 4, pp. 694–702, 2007.

Vandiver, J. K., Dimensionless parameters important to the prediction of vortex-induced vibration of long, flexible cylinders in ocean currents, Journal of Fluids and Structures, vol. 7, no. 5, pp. 423–455, 1993.

Versteeg, H. K., and Malalasekera, W., An introduction to computational fluid dynamics, 2nd ed., Pearson Education, 2007.

Wang, J., Zhang, Y., Liu, M., and Hu, G., Etching metasurfaces on bluff bodies for vortex-induced vibration energy harvesting, International Journal of Mechanical Sciences, vol. 242, p. 108016, 2023.

Zhao, M., Cheng, L., An, H., and Lu, L., Three-dimensional numerical simulation of vortex-induced vibration of an elastically mounted rigid circular cylinder in steady current, Journal of Fluids and Structures, vol. 50, pp. 292–311, 2014.

Biographies

Muhammad Jawad Zin Noor is a Mechanical Engineering alumnus (or former student) of KUET, Bangladesh. During his time at KUET, he was actively involved in extra-curricular engineering-related projects: for instance, he served as Suspension System Expert for a project team under KILO FLIGHT and did voluntary work under the KUET Automobile Club. Jawad is passionate about computational and experimental fluid mechanics, heat transfer and thermal management, and fluid-structure interaction. He is leaning towards more real-world applications of fluid mechanics and thermal management, especially in the field of product design, in a direction in which he is currently pursuing his career. Jawad is particularly passionate about bridging the gap between industry and academia.

Joy Ganguly was a student (or academic) in the Department of Mechanical Engineering at KUET, Bangladesh. During his time at KUET, he has developed a keen interest in mechanical design, fluid mechanics, and thermal systems. Alongside his academic coursework, Joy has been exploring how mechanical engineering principles can be leveraged for sustainable energy applications and industrial solutions. He is also interested in collaborative research and enjoys participating in team-based projects that combine theoretical learning with hands-on system modeling and experimentation. Joy aims to contribute to the development of efficient mechanical systems relevant to Bangladesh's industrial context.

Teertha Toran Chakraborty is a Mechanical Engineering graduate from Khulna University of Engineering and Technology (KUET) with 2.5 years of professional experience in the electric two-wheeler sector. He currently works as a Product Manager at Walton Digi-Tech Industries Ltd., where he leads electric bike product development, chassis manufacturing, production planning, and supply chain management. He is also a founding member of KUET's Formula Student team, responsible for designing and fabricating the car's intake and exhaust systems. His professional interests include electric vehicle technology, vibration and acoustic analysis, modal analysis, and advanced manufacturing processes.

© IEOM Society International

© IEOM Society International